ELSEVIER

Journal of Nuclear Materials 265 (1999) 91–99

journal of nuclear materials

Studies on hot hardness of Zr and its alloys for nuclear reactors

T.R.G. Kutty [a,*], K. Ravi [a], C. Ganguly [b]

[a] *Radiometallurgy Division, Bhabha Atomic Research Centre, Trombay, Mumbai 400 085, India*
[b] *Central Glass and Ceramic Research Institute, Jadavpur, Calcutta 700 032, India*

Received 29 November 1997; accepted 20 September 1998

Abstract

The hardness behaviour of pure Zr, Zircaloy 2, Zr–2.5Nb, Zr–2.5Nb–0.5Cu and Zr–1Nb–1Sn–0.1Fe alloys (composition in wt%) were evaluated from ambient temperature to 1173 K using a hot hardness tester in order to compare the hardness and to extract information on the strength behaviour from the hot hardness data using standard empirical relations. This paper summarizes the experimental hot hardness data of several Zr alloys and discusses the results with the help of their microstructure, alloy content and atomic radii of the constituents.

PACS: 62.20.Fe; 61.72.-y; 46.30.Pa

1. Introduction

Zirconium based alloys are the natural choice for both fuel element cans and in-core structural components in water-cooled nuclear reactors, since these alloys have low thermal neutron absorption cross section, adequate strength and ductility, good corrosion resistance, long-term dimensional stability in an irradiation environment, excellent compatibility with the fuel and coolant, good thermal conductivity and adequate resistance to fracture [1,2]. The most important alloy of Zr used in Pressurised Heavy Water Reactors (PHWRs) is Zircaloy (Zircaloy 2 and Zircaloy 4), which is commonly used for fuel cladding and also for pressure tubes and calendria tubes. In Zircaloy, the major alloying element is Sn. The addition of Sn lowers the stacking fault energy of Zr which is expected to have significant influence on workability [3,4] and creep strength. Zr–2.5Nb alloy is the new generation alloy for pressure tube material. Nb helps in improving the creep strength as well as oxidation and corrosion resistance. Zr–2.5Nb–0.5 Cu alloy is used for garter springs which separate the hot pressure tube from the cold calendria tube. The addition of Cu results in lowering the α–β transition temperature and partitions entirely to β-Zr. Cu is expected to modify the deformation characteristic of β alone in the $\alpha + \beta$ region [5]. The addition of Cu changes the ageing kinetics of the alloy. The quaternary Zr–1Nb–1Sn–0.1Fe alloy is an advanced cladding material which shows superior corrosion resistance and irradiation stability [6–8]. It has been reported that the irradiation creep and irradiation growth of the quaternary alloy is only 80% and 60%, respectively of that of Zircaloy 4 [8]. In a typical PHWR, the fuel tube sees a temperature of ~623 K and undergoes rigorous stress conditions due to pellet clad interaction. The pressure tube operates at ~558 K and has to withstand a coolant pressure of ~10 MPa. The garter spring should support the pressure tube initially and the creep sag subsequently and therefore should have adequate strength. Such a diverse range of specifications are met only through proper control of processing parameters [5]. It is worth investigating certain properties of Zr alloys such as hot hardness, since hardness is an easily measurable property and can be converted to the more useful strength data through well-established empirical relations. It may be noted that all the materials used in this study belonged to materials of various sizes and shapes making it practically impossible to resort to the conventional tension test. Hence, hardness testing methodology was used in order to

* Corresponding author. Tel.: +91-22 550 5319; fax: +91-22 550 5151; e-mail: rmd@magnum.barc.ernet.in

0022-3115/99/$ – see front matter
PII: S0022-3115(98)00610-2

derive the tensile strength from the hardness data. The hardness test method will also be a very useful tool for extracting information on the mechanical properties of irradiated Zr alloys since sample requirement for this test is very small. The only sample requirement of this test is a metallographically polished surface. This miniaturisation of the specimen reduces the induced radioactivity so that the testing can be carried out even outside the shielded cell. Instead of yielding one set of results on a specimen of many cm^2 surface, statistically significant number of results can be obtained per cm^2 surface using hardness tests [9]. Indentation testing technique, in particular microindentation method, can be regarded as a quick, simple and non-destructive mechanical procedure [9]. In this paper, the Zr alloys were compared in terms of their hot hardness in the temperature range of 293–1173 K. The hot hardness of the matrix material, pure Zr, has also been evaluated for comparison.

2. Experimental

The details of the samples used in this study, their heat treatment conditions and chemical composition are given in Tables 1 and 2. Samples were cut from the above mentioned alloys and were metallographically prepared. Hot hardness measurements were carried out using a hot hardness tester (Nikon, Model QM) with the help of a diamond Vickers pyramid indenter. Before starting the hot hardness experiment, the instrument was calibrated using a standard (Cu: SRM; National Bureau of Standards, USA) sample. Five indentations were made on the standard using 300 g load. The hardness obtained was found to be ±0.5% of the actual value. A load of 300 g and a dwell time of 5 s were used for this study. The load was applied at a rate of 0.2 mm/min. The hardness was measured in vacuum (0.1 Pa) from room temperature to 1173 K at every 100 K intervals. At each temperature, at least three readings were taken.

The hardness measurements were carried out on all alloys along the direction transverse to the axial direction. Fig. 1 schematically illustrates the plane and location on which hardness measurements were carried out. The strength and hardness of Zr and its alloys are strongly dependent on texture. Texture produced during the fabrication stage introduces anisotropy in mechanical properties. The development of texture during the forming operation is the direct result of different deformation mechanisms operating in Zr and its alloys. To reduce the effect of texture, the indentations were positioned in such a way that all of them had their diagonals parallel to a selected edge of the sample.

For microstructural examination, samples were cut from the alloys and were metallographically prepared. The etching has been carried out using a mixture of HF, HNO_3 and H_2O in the ratio 1:9:10. The microstructural details are presented in Table 1.

3. Results

The hardness (H) vs. temperature (T) plots for Zr, Zircaloy, Zr–2.5Nb, Zr–2.5Nb–0.5Cu and Zr–1Nb–1Sn–0.1Fe alloys are shown in Fig. 2. The H–T data of the above mentioned alloys were fitted by a polynomial and the equations for the best fit are given below:

Table 1
Details of samples used in this study

Material	Source of sample	Fabrication/heat treatment details	Microstructural details
Zr	Arc melted rod	Annealed at 1073 K for 15 min.	Grain size 25 μm, equiaxed grains.
Zircaloy 2	Fuel tube	β quenching, hot extrusion at 1073 K, cold pilgering, intermediate vacuum annealing at 1000 K, cold pilgering followed by final annealing at 773 K and autoclaving at 673 K for 24 h.	Single phase, slightly elongated grains with an average grain size of 15 μm. Typical parallel plate morphology at many places.
Zr-2.5Nb	Pressure tube	β quenching, hot extrusion at 1053 K, cold pilgering, intermediate vacuum annealing at 823 K, second pilgering followed by stress relieve anneal at 673 K for 24 h.	Two-phase structure. α and β phase stringers are elongated in the direction of extrusion. α is being enveloped by β phase.
Zr-2.5Nb-0.5Cu	Garter spring	β quenching, forging, hot rolling, hot swaging at 838 K, drawing and annealing at 838 K for 30 min., sandblasting, pickling and centreless grinding to the final dimension.	Two-phase structure consists of α Zr and β Nb. Widmanstatten morphology with prior β grain size around 80 μm.
Zr-1Nb–1Sn-0.1Fe	Received from NFC, Hyderabad	β quenching, hot extrusion, cold and hot rolling with intermediate vacuum annealing and final annealing at 973 K for 1 h.	Single phase, lath martensitic structure where α platelets are arranged in a typical basket weave morphology. width of the laths are 0.4–0.6 μm.

Table 2
Chemical composition of alloys

Material (wt%)	Sn	Nb	Fe	Cr	Ni	Cu	O (ppm)
Zr	–	–	–	–	–	–	1000
Zircaloy 2	1.3–1.6	–	0.07–0.2	0.05–0.15	0.03–0.08	–	1000–1300
Zr–2.5Nb	–	2.4–2.5	0.08–0.1	–	–	–	1000–1400
Zr–2.5Nb–0.5Cu	–	2.4–2.5	0.08–0.1	–	–	0.36–0.5	1000–1200
Zr–1Nb–1Sn–0.1Fe	1.08–1.15	1.10	0.098	0.018	–	–	1000–1200

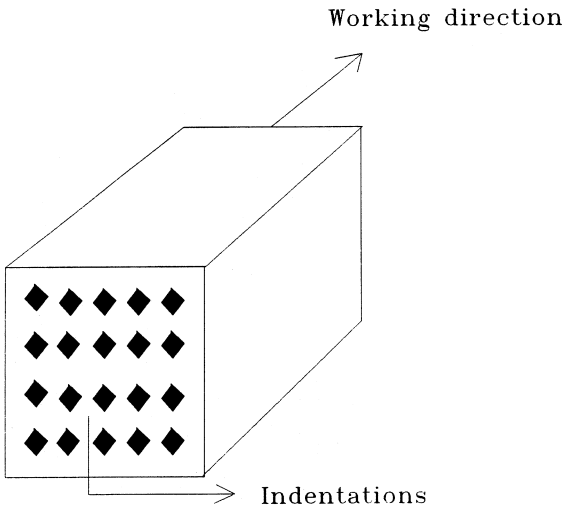

Fig. 1. A schematic showing plane and locations on which hot hardness measurements were made.

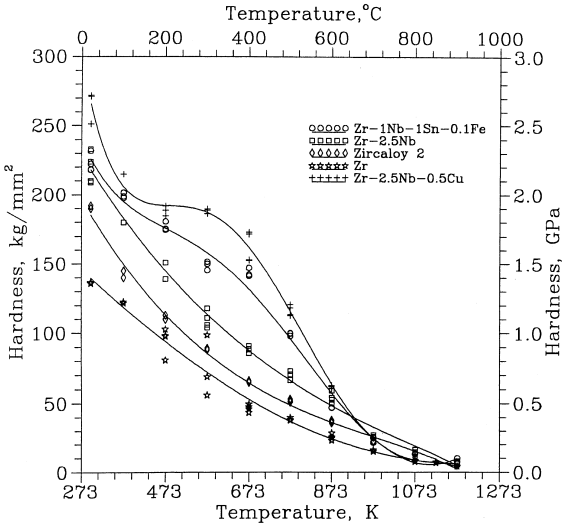

Fig. 2. Hardness vs. temperature plots for pure Zr, Zircaloy 2, Zr–2.5Nb, Zr–2.5Nb–0.5Cu and Zr–1Nb–1Sn–0.1Fe alloys from room temperature to 1173 K. The data of Zr, Zircaloy 2 and Zr–2.5Nb were best fitted using a third degree polynomial and that of Zr–2.5Nb–0.5Cu and Zr–1Nb–1Sn–0.1Fe alloys were fitted by a fifth degree polynomial.

Zr

$$H = 232.91 - 0.35T + 1.07 \times 10^{-4}T^2 + 2.19 \times 10^{-8}T^3, \quad (1)$$

Zircaloy 2

$$H = 390.56 - 0.92T + 8.39 \times 10^{-4}T^2 - 2.88 \times 10^{-7}T^3, \quad (2)$$

Zr–2.5Nb

$$H = 400.91 - 0.78T + 5.81 \times 10^{-4}T^2 - 1.76 \times 10^{-7}T^3, \quad (3)$$

Zr–2.5Nb–0.5Cu

$$H = 2164.18 - 15.17T + 0.045T^2 - 6.27 \times 10^{-5}T^3 + 4.13 \times 10^{-8}T^4 - 1.03 \times 10^{-11}T^5, \quad (4)$$

Zr–1Nb–1Sn–0.1Fe

$$H = 884.53 - 5.03T + 0.0142T^2 - 1.94 \times 10^{-5}T^3 + 1.21 \times 10^{-8}T^4 - 2.79 \times 10^{-12}T^5, \quad (5)$$

where H is in kg/mm^2 and T is in K.

It can be seen from Fig. 2 that the hardness values of Zr and Zr–2.5Nb–0.5Cu alloy are the lowest and highest, respectively, in the low temperature region up to 873 K. Zircaloy showed a considerable higher hardness than Zr at room temperature. The hardness–temperature curves of Zr–2.5Nb and Zircaloy 2, are almost parallel up to 1000 K, the hardness of Zr–2.5Nb alloy being higher than that of Zircaloy at all temperatures tested. The quaternary Zr–1Nb–1Sn–0.1Fe and ternary Zr–2.5Nb–0.5Cu alloys showed a different behaviour on heating. The hardness–temperature plots of these alloys showed a decrease in the softening in the temperature range of 373–673 K. For Zr–2.5Nb–0.5Cu alloy, the hardness in the temperature range of 373–573 K is almost constant.

The above data of Fig. 2 have been replotted using ln H vs. T and is shown in Fig. 3. The ln H–T plots for Zr and its alloys can be represented by two straight lines intersecting in the temperature range of 700–873 K. It was found that ln H vs. T plots for Zr, Zircaloy, Zr–2.5Nb are almost parallel up to the transition point. As mentioned earlier, Zr–2.5Nb–0.5Cu and Zr–1Nb–1Sn–0.1Fe alloys showed remarkable resistance for softening at low temperature below the transition. But above the

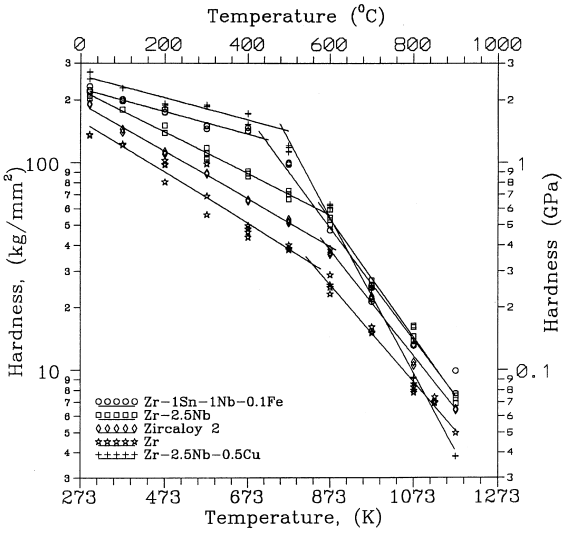

Fig. 3. ln(hardness) plotted against temperature (from room temperature to 1173 K) for Zr and its alloys. The transition points are also shown in the above figure.

transition temperature, the hardness of Zr–2.5Nb–0.5Cu alloy falls rapidly than the other alloys and its hardness is lowest at 1173 K.

4. Discussion

4.1. Hardness–temperature relation

The temperature dependence of hardness of metals and alloys has been reviewed by Westbrook [10]. The summary of his finding is that the temperature dependence of hardness is best represented by the following relation of the type

$$H = A\exp(-BT), \tag{6}$$

where constants A and B are called the intrinsic hardness (i.e. the value of hardness at 0 K) and softening coefficient, respectively. The constants A and B have one set of values at low temperature (A_I and B_I) and another at high temperature (A_{II} and B_{II}), suggesting a change of mechanism [11,12]. The value of A at low temperature is a measure of the inherent strength of the interatomic bond in the metal lattice and is related to the crystal structure and 'thermal energy of melting' which is defined as the heat content of the liquid metal at the melting point [10]. The constant B, which is the slope of ln H vs. T plot, indicates the rate at which the lattice is weakened by the thermal energy and is closely related to the coefficient of thermal expansion [13].

H–T data for Zr and its alloys shown in Fig. 3 can be fitted by the equation $H = A\exp(-BT)$. The values of the constants for low and high temperature regions are given in Table 3. The softening coefficient of Zr and Zr–2.5Nb–0.5Cu was highest and the lowest respectively below the transition temperature. The values of transition temperature (T_T) are also shown in Table 3 and was found to be lowest for Zr–1Nb–1Sn–0.1Fe alloy and highest for Zircaloy-2.

H–T data of Zr and its dilute alloys like Zr–Nb, Zr–Mo, Zr–Ti, Zr–U, Zr–Mo–Nb, Zr–Ti–Mo are available in the literature [14–18]. H–T curves of these alloys are similar to the one obtained in this study.

4.2. Transition temperature

From Table 3, it can be seen that transition temperature (T_T) of Zr alloys varies with composition. The transition temperature is a function of strain rate, purity and grain size. T_T has been identified as the manifestation of the onset of increased atomic mobility which permits dislocation atmosphere to diffuse to new sites within the time allowed by the test [19]. This temperature will be lower for lower strain rates because more time is available for the diffusion to take place. Those alloying elements that raise the α–β transformation temperature generally raise the T_T also. Among the alloying elements, Sn, Al, Hf etc., raise the transformation temperature while elements like Nb, Cr, Fe, Ni, Ti, Mo, Cu etc., lower it [18,20]. As expected addition of Sn has increased the transition temperature in the case of Zircaloy. But on the contrary, the addition of Nb has

Table 3
Values of constants A and B of the relation $H = A\exp(-BT)$

Alloy	A (kg/mm^2)		$B \times 10^{-3}$ (K^{-1})		Transition temperature, T_T (K)
	A_I	A_{II}	B_I	B_{II}	
Zr	347	2810	2.851	5.376	828
Zircaloy 2	397	6480	2.648	5.889	864
Zr-2.5Nb	417	16498	2.303	6.566	863
Zr-2.5Nb-0.5Cu	364	101879	1.218	8.636	755
Zr-1Nb–1Sn-0.1Fe	319	10937	1.256	6.209	713

A_I and A_{II} are the intrinsic hardness for low temperature ($293 < T < T_T$) and high temperature ($T_T < T < 1173$ K) regions, respectively. B_I and B_{II} are the softening coefficients for low and high temperature regions, respectively.

increased the transition temperature. This may be due to the strengthening effects of β phase which contain about 20 at.% of Nb. As both Nb and Cu lower the transformation temperature, a lower transition temperature is expected for Zr–2.5Nb–0.5Cu alloy which is found to be true for this study. The lowest T_T is obtained for Zr–1Nb–1Sn–0.1Fe alloy. The microstructure of this alloy consists of precipitates at lath boundaries. These precipitates control the flow behaviour in this alloy [7]. The coarsening of the precipitates results in rapid decrease in strength and results in lowering the transition temperature.

4.3. Correction for modulus

It is widely recognised that the flow stress of any metal consists of two components [21–23],

$$\sigma = \sigma^*(\epsilon, T) + \sigma_I(\dot{\epsilon}), \tag{7}$$

where σ^* is called the frictional or effective stress which depends on temperature and strain rate but not on the level of work hardening. σ^* becomes negligible at intermediate and high temperatures. In contrast, σ_I, the athermal stress, depends on temperature only through the temperature dependence of shear modulus [21]. σ^* is associated with the stress required in order to permit the glide dislocations to overcome the short range barriers by thermal activation where as σ_I is associated with long range elastic interaction of dislocations [24]. Since hardness and flow stress are intimately related, H can also be separated into rate dependent and rate independent components as:

$$H = H^*(\epsilon, T) + H_I(\epsilon), \tag{8}$$

where H^* represents the frictional component of hardness and H_I represents the athermal component, which is dependent on temperature through the temperature dependence of shear modulus. It is reported that the hardness and elastic properties of metals and alloys are closely related [10]. The Young's modulus of steel decreases by about 1/3 on heating up to 1073 K but a proportional reduction in hardness is of the order of 90% [25]. This indicates that the softening is associated with the reduction of modulus. To account for this, hardness–temperature data of Fig. 3 are replotted using modulus compensated hardness (H/G) and is shown in Fig. 4. The data can be represented by the relation similar to Eq. (6):

$$H/G = A_1 \exp(-B_1 T). \tag{9}$$

The values of the constants A_1 and B_1 are given in Table 4. The shear modulus (G) values at different temperatures are taken from the literature for Zr, Zircaloy and Zr–2.5Nb alloy (see Table 5) and used in this study [26–28]. Northwood et al., in Ref. [26] have shown that

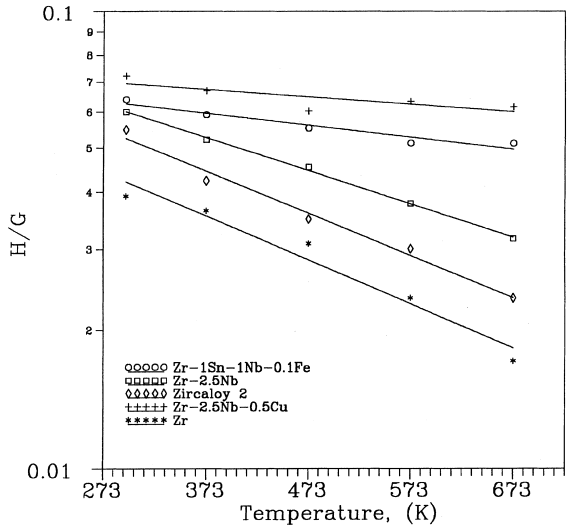

Fig. 4. A plot of modulus compensated hardness (H/G) against temperature (from room temperature to 673 K) for pure Zr, Zircaloy 2, Zr–2.5Nb, Zr–2.5Nb–0.5Cu and Zr–1Nb–1Sn–0.1Fe alloys. G is the shear modulus of the alloy. The average hardness values were used while plotting (H/G) vs. T.

modulus values do not change appreciably with the alloy additions. Hence the modulus values of Zircaloy have been used for Zr–2.5Nb–0.5Cu and Zr–1Nb–1Sn–0.1Fe alloys. The modulus correction has been given only for the low temperature ($T < 773$ K) data, since no reliable data on modulus are available for the high temperature up to 1173 K. On comparing Tables 3 and 4, it can be seen that the values of the softening coefficient (B) have

Table 4
Values of the constants of the relation $H/G = A_1 \exp(-B_1 T)$

Alloy	A_1	$B_1 \times 10^{-3}(K^{-1})$
Zr	0.0807	2.204
Zircaloy 2	0.0981	2.122
Zr-2.5Nb	0.0986	1.676
Zr-2.5Nb-0.5Cu	0.0782	0.391
Zr-1Nb–1Sn-0.1Fe	0.0748	0.607

Table 5
Shear modulus values of Zr, Zircaloy 2 and Zr–2.5Nb alloys at different temperatures [32,34]

Temperature (K)	Shear modulus (GPa)		
	Zr	Zircaloy 2	Zr–2.5Nb
293	34.0	34.8	35.9
373	31.6	33.6	34.5
473	29.3	31.8	31.2
573	26.9	29.4	29.6
673	24.6	27.9	27.1

decreased on giving correction for modulus. The maximum decrease in the value of softening coefficient (B) was found to be for Zr–2.5Nb–0.5Cu followed by Zr–1Nb–1Sn–0.1Fe alloy.

4.4. Effect of alloying elements on hardness

Chubb et al., in Refs. [14–16] have reported that the alloying elements increase the hardness of Zr at all temperatures. It is reported that Nb is more effective in strengthening Zr than Sn up to 773 K. It is found that hardness of Zr–Nb alloys falls considerably above 873 K [18,19]. The decrease in hardness with increase in temperature is greater for Zr–Nb alloys than Zr–Sn alloys above 773 K and therefore strengthening effect of Sn at high temperature is greater than that of Nb. Cu is found to be superior than Nb in strengthening Zr alloys at low temperature. The above observations have also been found to be true for the alloys investigated in this study on comparing the values of softening coefficients given in Table 3.

Apart from the addition of alloying elements, the hardness is affected in these alloys by cold work and texture [1]. The various strengthening mechanisms operating in Zr alloys have been reviewed in the literature [1,2,4]. Solid solution hardening by both substitutional and interstitial elements is always observed in Zr alloys. However this is possible only to a limited extent because of low solubility of the common alloying elements such as Fe, Cr, Ni etc., in α-Zr. The most potent interstitial solution hardening agent is O. N also acts quite similar to O. Many of the Zr alloys are hardenable through martensitic transformation. The effect of alloying elements on strengthening and deformation behaviour is discussed below.

As mentioned earlier, the major alloying element in Zircaloy 2 is Sn. Sn has an atomic radius which is very close to Zr as shown in Table 6. The mechanism of hardening of Zircaloy by Sn is by solid solution hardening. Hardening in Zircaloy also occurs due to the formation of intermetallics, namely $Zr(Fe,Cr)_2$ and $Zr_2(Fe,Ni)$ [30]. Wadekar et al., in Ref. [29] have evaluated the yield and ultimate tensile strength of Zr–Sn alloys as a function of tin content. The 0.2% yield strength showed a linear relationship with $c^{2/3}$, where c is the concentration of tin. This suggests a Mott and Nabarro model of solid solution strengthening in which clustering of solute atom is envisaged. The effect of tin content on yield strength at temperatures between 77 K and 673 K has also been reported in Ref. [29]. The data indicate that the addition of tin has influenced both the thermal and the athermal component of the flow stress. The rate controlling mechanism of softening in binary Zr–Sn alloy at temperatures below 473 K involves the dislocations overcoming the obstacles provided by random pinning of tin atoms. At temperatures above 473 K the mechanism appears to be controlled by the movement of jogged screw dislocations [29].

Table 6
Atomic radii of Zr and other alloying elements

Element	Atomic radius (Å)	Difference in atomic radius with that of Zr (%)
Zr	1.60	–
Nb	1.47	8.1
Sn	1.58	1.3
Fe	1.28	20
Ni	1.25	22
Cr	1.28	20
Cu	1.28	20

The hardness of Zr–2.5Nb alloy is higher than that of Zircaloy from room temperature to 1173 K (see Fig. 2). It is reported that Nb is more effective in increasing the yield strength in Zr than a comparable amount of Sn [32]. Nb stabilizes the β phase of Zr. The atomic diameter of Nb is smaller than that of Zr (Table 6) and therefore produces considerable strengthening in Zr–2.5Nb alloy. Zr–2.5Nb alloy is basically a two-phase system. The distribution and composition of α and β phases are strongly influenced by the hot working parameters. The microstructural parameters such as volume fraction of the phases, thickness and aspect ratio of α and β stringers and dislocation structure of α grains vary during each stage of the fabrication [31]. The microstructure of pressure tube after final heat treatment consists of α and β phase stringers elongated in the direction of extrusion, the former being enveloped by the latter. The α grains are shaped like elongated platelets containing about 1 at.% Nb with high density of dislocation network. They are stacked together and separated by β phase containing ~20 at.% Nb. The dislocation density in α grains is estimated to be 15×10^{12} lines/cm^2 [31]. The formation of Zr_2Fe intermetallic also contributes to hardening in this alloy. The temperature dependence of yield strength of Zr–2.5Nb pressure tube has been studied by Singh et al., in Ref. [33]. They have indicated a plateau and a peak region between 523–573 K, indicating a possible occurrence of dynamic strain ageing at these temperatures. Such plateau have not been observed in H–T plot in this study. The relatively higher strain rate involved in the hardness testing compared to the conventional tension test could be the cause for the non-appearance of plateau in the H–T plot.

Zr–1Nb–1Sn–0.1Fe alloy exhibits a higher hardness than Zircaloy and Zr–2.5Nb alloy below the transition temperature [34]. β quenching of this alloy produces a single phase lath martensite where α plates are arranged in typical basket-weave morphology. The laths were reported to contain high dislocation density (10^{13} lines/cm^2) [7]. On aging this alloy at 973 K resulted in the distribution of precipitates at lath boundaries. Wadekar

et al., in Ref. [7] have conducted a detailed study on structure property correlations of the above mentioned alloy and reported that the highly supersaturated β quenched alloy is not a homogeneous solid solution but contains a distribution of very fine Nb rich clusters which controls the flow behaviour. On ageing, the precipitates decorate the lath boundaries which act as a strong barrier for dislocations. The formation of Zr_2Fe phase helps in further strengthening this alloy. The high dislocation density and precipitates resulted in a higher hardness in this alloy.

The highest hardness obtained in this study was for Zr–2.5Nb–0.5Cu alloy. The addition of 0.5Cu to Zr–2.5Nb alloy has been reported to increase the hardness of martensite α by 35% [35]. This strengthening has been attributed mainly to solid solution hardening of α by copper. The atomic radius of copper is about 20% lower than that of Zr. This lower atomic diameter of Cu imparts remarkable hardness thereby strengthening this alloy. The secondary hardening of the matrix occurs due to β-Nb precipitates at twin and grain boundaries [35,36]. The low softening coefficient obtained for this alloy is due to these hardening processes. Aging of this alloy above 773 K has resulted in a decrease in hardness [37]. This decrease in hardness is attributed to overaging which resulted in a steep decrease in the value of the softening coefficient.

4.5. Correlation between hardness and strength

The following relations have been reported for Zr and its alloys relating hardness and strength [16]:

$$\sigma_y = 0.155H, \tag{10}$$

$$\sigma_{UTS} = 0.218H, \tag{11}$$

where H and σ are in kg/mm^2. Kapoor et al., in Ref. [37] have proposed a relation between ultimate tensile strength (σ_{UTS}) and hardness for Zr–2.5Nb alloy which is given below:

$$H = (\sigma_{UTS} \times 341.6)/(\sigma_{UTS} + 42.05), \tag{12}$$

where values of σ_{UTS} and H are in kg/mm^2. The σ_{UTS} values obtained from the work of Singh et al., in Ref. [33] and the hardness data determined in this study were substituted in Eq. (12) for ascertaining its validity since both the types of data emerged from the same source, namely Zr–2.5Nb alloy pressure tube. This exercise clearly demonstrated that the above equation was valid only for room temperature. Similarly Eqs. (10) and (11) are not found satisfactory to correlate hardness and tensile strength. Hence, Eqs. (10)–(12) cannot be considered as a general equation having applicability in covering a wide range of temperatures.

Fig. 5 shows the variation of hardness and σ_{UTS} with temperature for Zircaloy 2 and Zr–2.5Nb alloy. σ_{UTS} values are taken from the literature [2,5,8,33]. Since the above data are from the same material, a correlation between hardness and σ_{UTS} is attempted. The relation thus obtained for Zr–2.5Nb and Zircaloy 2 are given below respectively:

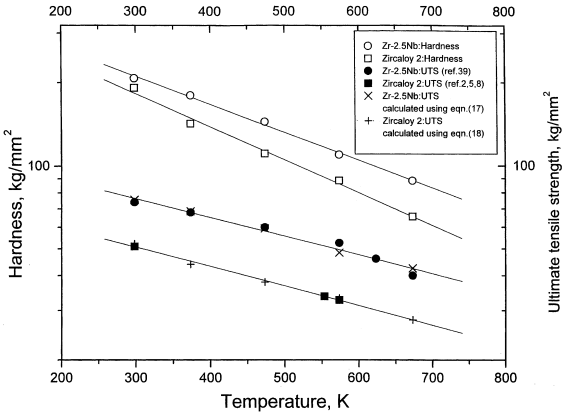

Fig. 5. ln(hardness) and ln σ_{UTS} vs. temperature plot for Zr–2.5Nb and Zircaloy 2. The open symbols are hardness data and closed symbols are strength data. The (×) and (+) symbols are the fitted data for Zr–2.5Nb and Zircaloy 2 respectively using Eqs. (17) and (18).

$$\ln \sigma_{UTS} = 0.676 \ln H + 0.7197, \tag{13}$$

$$\ln \sigma_{UTS} = 0.590 \ln H + 0.8562. \tag{14}$$

The values of σ_{UTS} obtained using Eqs. (13) and (14) are also shown in Fig. 5 and it can be seen that the above relations are quite adequate to predict the values of σ_{UTS} from hardness data for a temperature range of 273 to 673 K.

4.6. Mechanism of softening

The mechanisms of softening in metals and alloys at low and high temperatures are widely discussed in the literature [10–13,38–40]. At low temperature below 0.5 T_m, hardness is a weak function of temperature and plastic deformation occurs mainly by athermal mechanisms. The major mode of deformation is by slip along preferred planes and directions. The other mechanisms for softening at low temperature during the hardness testing are as given below [38]:

1. Since local stresses under the indenter are comparable to theoretical elastic limit, they are sufficiently high to create dislocations in an ideal crystal. Thus indentation generates prismatic loops of dislocation in the crystal which are successfully removed from the indentation region by conservative climb process [41].
2. Densification of the crystal structure by transition to a dense, metallic phase under action of large hydrostatic compression under the indenter [42].

3. Stress activated dislocation glide by nucleation and lateral propagation of double kinks, which necessitates the breaking of atomic bonds.
4. Deformation twinning.

The mechanisms proposed for softening at high temperature above the transition are diffusional phenomena such as dislocation climb and glide processes.

α-Zr has a hexagonal close-packed structure with c/a ratio less than the ideal. Because of the limited number of primary slip systems and their non-symmetric distribution, α-Zr deforms both by slip and twinning. In the temperature range from room temperature to 773 K, the rate controlling deformation mode in pure Zr under compression is seen to change from twinning at low temperature to slip at high temperature [43]. In the above temperature range, α-Zr deforms by slip mostly on $\{1\ 0\ \bar{1}\ 0\}$ first order prism planes along $\langle 1\ 1\ \bar{2}\ 0\rangle$ direction. Slip has also been reported to occur on basal plane $\{0\ 0\ 0\ 1\}$ along $\langle 1\ 1\ \bar{2}\ 0\rangle$ direction. Pyramidal slip on $\{1\ 0\ \bar{1}\ 1\}$ has been observed at sites of stress concentration. It has been suggested that the prismatic slip is favoured over the basal slip in view of the lower stacking fault energy associated with prism planes compared to other slip planes. However, incidence of basal slip has been found to increase with increasing temperature [4,43,44].

Apart from slip, twinning plays a major role in the deformation of α-Zr as an alternative to slip, and in the evolution of texture in Zr during deformation [4]. Various types of twins have been observed during deformation of Zr: $\{1\ 0\ \bar{1}\ 2\}\ \langle 1\ 0\ \bar{1}\ 1\rangle$ and $\{1\ 1\ \acute{2}\ 1\}\ \langle 1\ 1\ \bar{2}\ 6\rangle$ in tension and $\{1\ 1\ \bar{2}\ 2\}$ in compression. At elevated temperature, $\{1\ 0\ \bar{1}\ 1\}$ and $\langle 1\ 0\ \bar{1}\ 2\rangle$ twinning has been reported. The $\{1\ 1\ \bar{2}\ 1\}$ twins have been found to be dominant at all temperatures. Hence slip and deformation twinning are the mechanism of softening of Zr and its alloys at low temperature below the transition, slip being dominant above the room temperature. The other rate controlling mechanisms of softening at temperatures below the transition are due to dislocations overcoming the obstacles provided by random pinning of solute atoms and by the movement of jogged screw dislocations. The enhanced plasticity observed in Zr alloys above transition temperature is due to the following:

- occurrence of cross slip,
- possible activation of basal slip and,
- ease of operation of pyramidal slip.

The thermally activated processes such as dislocation glide or a mixture of climb–glide process also play a major role in the softening process in these alloys.

5. Conclusions

The hardness of Zr-based alloys used in nuclear thermal reactors was measured from ambient temperature to 1173 K and the following conclusions were drawn:

1. The hardness of Zr and Zr–2.5Nb–0.5Cu alloy was the lowest and the highest respectively in the low temperature region below the transition. The effect of alloying elements like Cu, Nb, Sn has been discussed and found that Cu followed by Nb are the best strengthening agents in Zr.
2. The hardness–temperature behaviour of these alloys can be explained in terms of their microstructure, alloy content and atomic radii of the constituents.
3. A correlation between hardness and σ_{UTS} has been established for Zircaloy 2 and Zr–2.5Nb alloy for a temperature range of 273 to 673 K.

Acknowledgements

The authors wish to acknowledge Mr D.S.C. Purushotham, Head, Radiometallurgy Division, for permitting to publish this work and for his keen interest in this research programme. They wish to record their sincere thanks to Dr S. Banerjee, Head, Materials Science Division for reviewing this paper and for useful suggestions. The suggestions rendered by Messrs K.C. Sahoo, S. Anantharaman, K.S. Balakrishnan and Dr J.K. Chakravarthy are kindly acknowledged.

References

[1] D.G. Franklin, G.E. Lucas, A.L. Bement, in: ASTM-STP-815, ASTM, Philadelphia, 1983, p. 16.
[2] P. Rodriguez, Proceedings of Zirconium Alloys for Reactor Components (ZARC-91), Bombay, India, 12–13 December 1991, Department of Atomic Energy, Bombay, 1991, p. 46.
[3] W.A. McInteer, D.L. Baty, K.O. Stein, in: ASTM-STP-1023, ASTM Philadelphia, 1989, p. 621.
[4] C. Lemaignan, A.T. Motta, in: B.R.T. Frost (Ed.), Materials Science and Technology, Vol. 10B, VCH, Weinheim, 1994, p. 1.
[5] J.K. Chakravarthy, in Optimization of Hot Workability and Control of Microstructure in Zirconium and Zirconium Alloys using Processing Maps, PhD thesis, Indian Institute of Science, Bangalore, 1992, p. 4.
[6] G.P. Sabol, G.R. Kilp, M.G. Balfour, E. Roberts, in: ASTM-STP-1023, ASTM, Philadelphia, 1989, p. 227.
[7] S.L. Wadekar, S. Ganguly, G.K. Dey, J.K. Chakraborthy, V. Chopra, P. Pande, in: S. Banerjee, R.V. Ramanujan (Eds.), Proceedings of International Conference on Physical Metallurgy ICPM-94, Bombay, India, 9–11 March 1994, Gordon and Breach, Amsterdam, 1996, p. 443.
[8] K. Balaramamurthy, Proceedings of Zirconium Alloys for Reactor Components (ZARC-91), Bombay, India, 12–13 December 1991, Department of Atomic Energy, Bombay, 1991, p. K-1.
[9] Hj. Matzke, Europian Applied Research Report EUR-10597, vol. 7, 1987, p. 13.

[10] J.H. Westbrook, Trans. Am. Soc. Met. 45 (1953) 221.
[11] H.D. Merchant, G.S. Murthy, S. Bahadur, L.T. Dwivedi, Y. Mehrotra, J. Mater. Sci. 8 (1973) 437.
[12] A.G. Atkins, D. Tabor, Proc. Royal. Soc. A 292 (1966) 441.
[13] E.R. Petty, H. O'neill, Metallurgia 63 (1961) 25.
[14] W. Chubb, G.T. Muehlenkamp, G.T. Manning, Battelle Memorial Institute Report BMI-987, 1955.
[15] W. Chubb, G.T. Muehlenkamp, A.D. Schwope, Battelle, Memorial Institute Report BMI-833, 1953.
[16] W. Chubb, G.T. Muehlenkamp, F.R. Shober, A.D. Schwope, in: B. Lustman, F. Kerzer Jr. (Eds.), Metallurgy of Zr, McGraw Hill, New York, 1955, p. 490.
[17] A.D. Schwope, W. Chubb, J. Met. 4 (1952) 1138.
[18] W. Chubb, Trans. Am. Soc. Met. 48 (1956) 804.
[19] A. Salnas-Rodriguez, M.G. Akben, J.J. Jonas, E.F. Ibrahim, Can. Met. Quart. 24 (1985) 259.
[20] R.J. Van Thyne, D.J. McPherson, Trans. Am. Soc. Met. 48 (1956) 795.
[21] D.S. Stone, K.B. Yoder, J. Mater. Res. 9 (1994) 2524.
[22] G. Taylor, Prog. Mater. Sci. 36 (1992) 29.
[23] O.D. Sherby, P.E. Armstrong, Metall. Trans. 2 (1971) 3479.
[24] H. Mughrabi, in: R.W. Cahn, P. Haasen, E.J. Krammer (Eds.), Materials Science and Technology, vol. 6, VCH, Weinheim, 1993, p. 10.
[25] G.E. Geach, Int. Met. Rev. 19 (1974) 255.
[26] D.O. Northwood, I.M. London, H.L. Bahen, J. Nucl. Mater. 55 (1975) 299.
[27] P.E. Armstrong, H.L. Brown, Trans. AIME. 230 (1964) 962.
[28] W.J. Duffin, F.A. Nicholas, J. Nucl. Mater. 45 (1972/73) 302.
[29] S.L. Wadekar, S. Banerjee, V.V. Raman, M.K. Asundi, in: C.M. Eucken, A.M. Garde (Eds.), ASTM-STP-1132, Zirconium in the Nuclear Industry, ASTM, Philadelphia, PA, 1991, p. 140.
[30] A.M. Olmedo, J. Mater. Sci. 15 (1980) 1050.
[31] D. Shrivastawa, S. Banerjee, Proceedings of Zirconium Alloys for Reactor Components (ZARC-91), Bombay, India, 12–13 December 1991, Department of Atomic Energy, Bombay, 1991, p. 228.
[32] D.L. Douglass, J. Nucl. Mater. 9 (1963) 252.
[33] R.N. Singh, R. Kishore, G.K. Dey, T.K. Sinha, in: S. Banerjee, R.V. Ramanujan (Eds.), Proceedings of International Conference on Physical Metallurgy (ICPM-94), Bombay, India, 9–11 March 1994 (Eds.), Gordon Breach, Amsterdam, 1996, p. 451.
[34] T.R.G. Kutty, T. Jarvis, C. Ganguly, J. Nucl. Mater. 246 (1997) 189.
[35] K. Tangri, M. Chaturvedi, Trans. AIME 245 (1969) 991.
[36] J.K. Chakravarthy, G.K. Dey, S. Banerjee, Y.V.R.K. Prasad, J. Nucl. Mater. 218 (1995) 247.
[37] K. Kapoor, K.M. Sreedharan, A. Lakshminarayana, J.S. Kumar, V.A. Chandramouli, Proceedings of Zirconium Alloys for Reactor Components (ZARC-91), Bombay, India, 12–13 December 1991, Department of Atomic Energy, Bombay, 1991, p. 420.
[38] M.G.S. Naylor, T.F. Page, J. Microsc. 130 (1983) 345.
[39] T.O. Mulhearn, D. Tabor, J. Inst. Met. 89 (1960, 1961) 7.
[40] D. Tabor, in: P.J. Blau, B.R. Lawn (Eds.), Microindentation Technique in Materials Science and Eng., ASTM-STP-889, ASTM, Philadelphia, PA, 1985, p. 129.
[41] T. Figielski, Phys. Stat. Sol. 4A (1971) 773.
[42] I.V. Gridneva, Yu.V. Milman, V.I. Trefilov, Phys. Stat. Sol. 14A (1972) 177.
[43] S.G. Song, G.T. Gray, Metall. Trans. 26A (1995) 2665.
[44] D.L. Douglass, in: The Metallurgy of Zirconium, IAEA, Vienna, 1971, p. 41.